Tribol Lett (2011) 41:83–95
DOI 10.1007/s11249-010-9687-0

ORIGINAL PAPER

In Situ Studies of Cartilage Microtribology: Roles of Speed and Contact Area

E. D. Bonnevie · V. J. Baro · L. Wang · David L. Burris

Received: 28 May 2010 / Accepted: 10 August 2010 / Published online: 1 September 2010

Abstract The progression of local cartilage surface damage toward early stage osteoarthritis (OA) likely depends on the severity of the damage and its impact on the local lubrication and stress distribution in the surrounding tissue. It is difficult to study the local responses using traditional methods; in situ microtribological methods are being pursued here as a means to elucidate the mechanical aspects of OA progression. While decades of research have been dedicated to the macrotribological properties of articular cartilage, the microscale response is unclear. An experimental study of healthy cartilage microtribology was undertaken to assess the physiological relevance of a microscale friction probe. Normal forces were on the order of 50 mN. Sliding speed varied from 0 to 5 mm/s, and two probes radii, 0.8 and 3.2 mm, were used in the study. In situ measurements of the indentation depth into the cartilage enabled calculations of contact area, effective elastic modulus, elastic and fluid normal force contributions, and the interfacial friction coefficient. This work resulted in the following findings: (1) at high sliding speed ($V = 1$–5 mm/s), the friction coefficient was low ($\mu = 0.025$) and insensitive to probe radius (0.8–3.2 mm) despite the fourfold difference in the resulting contact areas; (2) the contact area was a strong function of the probe radius and sliding speed; (3) the friction coefficient was proportional to contact area when sliding speed varied from 0.05 to 5 mm/s; (4) the fluid load support was greater than 85% for all sliding conditions (0% fluid support when $V = 0$) and was insensitive to both probe radius and sliding speed. The findings were consistent with the adhesive theory of friction; as speed increased, increased effective hardness reduced the area of solid–solid contact which subsequently reduced the friction force. Where the severity of the sliding conditions dominates the wear and degradation of typical engineering tribomaterials, the results suggest that joint motion is actually beneficial for maintaining low matrix stresses, low contact areas, and effective lubrication for the fluid-saturated porous cartilage tissue. Further, the results demonstrated effective pressurization and lubrication beneath single asperity microscale contacts. With carefully designed experimental conditions, local friction probes can facilitate more fundamental studies of cartilage lubrication, friction and wear, and potentially add important insights into the mechanical mechanisms of OA.

Keywords Cartilage · In situ · Contact mechanics · Microtribology

List of symbols

A	Contact area
a	Contact area half-width
δ_s	Sample indentation depth
E_0	Equilibrium elastic modulus
E'	Effective elastic modulus
F_e	Elastic force component
F_f	Friction force
F_n	Normal force (measured)
F_p	Fluid pressure force component
H_a	Aggregate modulus
K	Permeability
Pe	Peclet number
R	Radius of spherical contact probe

E. D. Bonnevie · V. J. Baro · L. Wang · D. L. Burris (✉)
Department of Mechanical Engineering, University of Delaware, Newark, DE 19716, USA
e-mail: dlburris@udel.edu

μ Friction coefficient
V Speed of cartilage reciprocation
z Vertical stage displacement

1 Introduction

Osteoarthritis (OA), the leading cause of severe disability in the United States [1], is characterized by the initiation and progression of cartilage damage. While the causes of OA remain unclear, mechanical factors (e.g., altered joint loading) have been linked to OA risk [2]. On the micro- and cellular scale, the cartilage surface is continuously damaged and repaired [3]. The accumulation of damage prior to complete recovery can destabilize the system; further, if the damage interferes with lubrication, elevated stresses may propagate the damage to the surrounding tissue. There is presently little understanding of the potential feedback interactions between lubrication, stress and damage. Microtribological studies have the potential to clarify the mechanical aspects of OA.

Decades of research have targeted the macroscale load bearing and lubrication mechanisms responsible for the unusual tribology and durability of articular cartilage. The biphasic theory of cartilage mechanics accurately predicts the experimentally observed response of cartilage to a number of simple loading conditions and, as a result, has gained wide acceptance as an appropriate constitutive model for cartilage [4, 5]. Essentially, a nanoporous matrix provides load support via elastic deformation, while simultaneously serving to resist the flow of an interstitial fluid. The pressure gradient, according to Darcy's law, is proportional to the flow rate and inversely proportional to the permeability (a measure of ease of flow). The resulting fluid pressure (distribution) can support a substantial fraction of the load (90–99% in typical conditions) during deformation, thereby reducing the normal and traction stresses carried by the soft matrix [6]. Ateshian [7] reviewed the current state of cartilage tribology in 2009.

A number of cartilage lubrication theories have been proposed; the most notable are hydrodynamic [8–10], squeeze film [9, 10], hydrostatic (weeping) [4, 11], boundary [12–15], elastohydrodynamic [16], boosted [17, 18] and combinations thereof. McCutchen [4] slid a cartilage plug over a relatively large lubricated flat and found that friction was initially extremely low and increased with time. This effect has been independently reproduced numerous times since [19–21]. The time-dependent response is generally characterized by an initial friction coefficient ($\mu < 0.01$), a characteristic time constant and an equilibrium friction coefficient ($\mu_{eq} \sim 0.2$) [21]. Krishnan et al. [19] showed that the phenomenon was due to the time-dependent evacuation of pressurized fluid and the subsequent increase in the load supported by the solid. This effect has induced questions (as recently as 2008) as to whether or not low friction is sustainable in vivo [4, 18, 21]. Walker et al. [18] proposed that a combination of fluid film lubrication during unloaded swing, squeeze film lubrication during compression and boosted lubrication (where trapped pools of synovial fluid are left once the water vacates the contact) during sliding could sustain low friction. McCutchen [4] used a simple poroelastic model (with the same physical underpinnings as the biphasic model) to show that the time constant for fluid pressure loss was proportional to the contact area. He noted the relatively larger contact areas in the body and suggested that long time constants and opportunities for rehydration during intermittent unloading were sufficient to maintain low friction in vivo.

In 2006, Bell et al. [22] observed sustainable low friction when cartilage was slid against cartilage. In 2008, Caligaris et al. [21] achieved sustained lubrication ($\mu \sim 0.01$) using a spherical glass slider against a cartilage flat and confirmed a prediction by Wang and Ateshian [23] that fluid pressurization can be maintained during rolling and plowing. These results suggest that unloading events and multiple synergistic lubrication mechanisms are unnecessary for sustained low friction.

The distinction between sustainable lubrication and time-dependent lubrication is important. When Caligaris et al. [21] inverted the experiment and slid a cartilage sample against a larger glass flat, they observed a lower initial friction coefficient ($\mu \sim 0.001$) followed by a monotonic increase in friction with time up to $\mu \sim 0.2$. This simple experiment provides significant insights into the lubrication of cartilage. Darcy's law requires a constant flow rate for constant pressurization. As fluid leaves a *stationary* contact over time, the deformation rate, flow rate, and pressure approach zero. When the contact area *migrates* across the cartilage surface, hydrated cartilage is continuously introduced into the contact providing the necessary fluid for pressurization. The pressurized fluid within the contact preferentially flows into the depleted post-contact zone to rehydrate it for subsequent loading. This migration process gives sustainable pressurization and lubrication. Caligaris et al. [21] have called these stationary and migrating contacts, respectively.

Ateshian and Wang predicted that fluid load support (the fraction of the total normal force supported by pressurized fluid) and lubrication effects deteriorate with reduced speed and contact radius [23, 24]. Caligaris et al. [21] tested this prediction by varying speed and probe radius under migrating conditions. For a bovine femoral condyle against the mating tibial plateau, they observed increased friction with decreased velocity; a migrating contact is a necessary

but insufficient condition for sustained low friction. Glass lenses of 6.5 and 13 mm radii were also tested against the tibial plateau; the friction coefficient tended to increase with reduced probe radius, but the results were deemed statistically insignificant. They proposed that fluid load support occurs when the deformation rate is greater than the diffusive velocity (characteristic flow rate), or when the Peclet number (*Pe*) is greater than 1. The Peclet number was defined as the product of sliding velocity and cartilage thickness (or contact half-width) divided by the product of aggregate modulus and permeability.

Park et al. [25] probed the microscale tribological response of cartilage using an atomic force microscope (AFM) with a 5 μm polystyrene tip in a migrating contact. The friction coefficient began and remained high ($\mu \sim 0.15$) for each of the measurements. The authors suggested that the microscale contact was too small to provide pressurization and determined that microscale contacts offered a unique opportunity to study boundary friction of cartilage in the absence of fluid pressurization. Upon discovery of the migrating contact effect 4 years later, Caligaris et al. [21] revisited the migrating AFM results and estimated a contact radius of 1 μm and Peclet number of 0.1. These results were consistent with the hypothesis that $Pe = 1$ represents a limiting condition for fluid pressurization and lubrication.

To date, physiologically relevant fluid pressurization has not been demonstrated under a microscale contact involving cartilage. By definition, the friction force beneath a macroscopic friction probe represents the sum of many microscale interactions within a larger area of contact. Any interesting local effects from cellular structure, topography or initial surface damage (e.g., at the onset of OA) are attenuated by the effects of the larger healthy areas. This work is an exploratory study of cartilage tribology at a length-scale approaching that of the surface damage typical of early OA. The primary objectives were to: (1) measure the effect of velocity and probe radius on friction; (2) measure contact areas in situ; (3) determine the relationship between speed, effective modulus, contact area, solid load support, and friction; and (4) demonstrate sustainable fluid pressurization beneath a localized contact and establish a path forward for more fundamental studies of cartilage friction, stress, lubrication, and wear.

2 Experimental

2.1 Materials

Adult bovine cartilage was used for the study; cartilage explants were taken from lateral femoral condyles of adult animals (12- to 20-month old) obtained from a local butcher.

While the surfaces and properties of engineering materials can be carefully controlled to mitigate sample to sample variability, no such control is available for biological materials which are known to exhibit marked property variations between animals, across a single surface [26] and over time as the material breaks down. Preliminary tests were carried out to determine the sample to sample, spatial and time-dependent variability of bovine articular cartilage. Significant changes in mechanical properties due to time-dependent degradation were always observed after 5 days of refrigerated aging in PBS at 34 °F; no significant changes were ever observed within 24 h of extraction. The indentation force varied by as much as 50% at a single set of conditions for varying locations along the femoral condyles of more than 10 independent animals. Spatial variations over a single ∅10 mm sample were rarely significant, and testing on a single spot always offered excellent repeatability. All of the measurements reported here were collected at one location in the center of one representative sample within 8 h of extraction to minimize the influence of varied material properties on the results.

Following disarticulation, a ∅10 mm × 10 mm (approximately 1 mm cartilage, 9 mm bone) cylindrical sample was obtained using a hole-saw. Following extraction, the sample was rinsed, mounted and submerged in phosphate buffered saline (PBS). The sample was allowed to equilibrate prior to testing. Spherical 440C stainless steel probes of less than 30 nm average roughness (measurements were made with a scanning white-light interferometer over a 400 × 600 μm^2 field of view) had average radii of 0.8 and 3.2 mm.

2.2 Tribometer

The primary features of the tribometer used in this study are illustrated in Fig. 1. The tribometer was custom designed for normal forces on the order of 10–100 mN. A 2-axis translation/tilt stage enables coarse positioning of the sample relative to the probe and angular alignment of the sample with respect to the transducer. As Caligaris et al. pointed out, cartilage surfaces are macroscopically curved which makes alignment impossible [21]. As Schmitz et al. [27] showed, the measured friction coefficient is:

$$\mu^* = \frac{\mu\cos(\alpha) - \sin(\alpha)}{\cos(\alpha) + \mu\sin(\alpha)} \quad (1)$$

where μ^* is the measured friction coefficient, μ is the true friction coefficient, and α is the angle between the cartilage surface normal at the contact and the z-axis of the force transducer. For typical samples of cartilage, measurement bias from 100 to 1000% will be obtained (e.g., $\mu = 0.01$, $\alpha = 1°$, $\mu^* = 0.027$). Caligaris et al. [21] used active control (similar to an AFM) to determine the surface

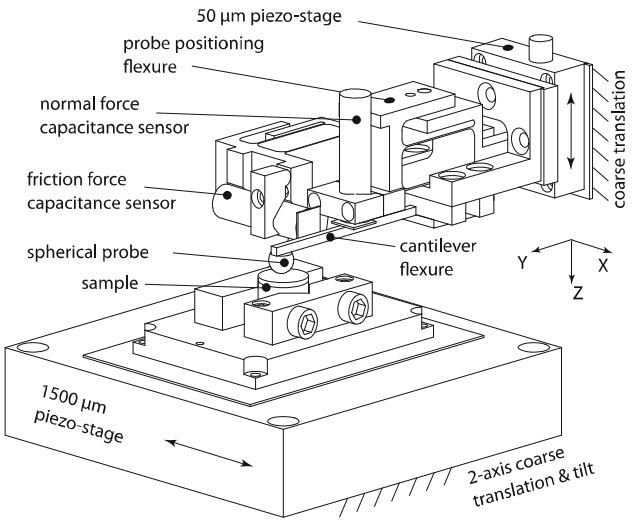

Fig. 1 Illustration of the custom microtribometer. A piezoelectric direct-metrology nanopositioning stage indents at a prescribed rate to a set z distance. A horizontal nanopositioning stage imposes a reciprocation motion at a prescribed speed over a 1500 µm track. Capacitance measurements of stage and transducer deflections are used to determine the sample indentation depth and force response in the *X* and *Z* directions

topography during the measurement and mathematically solve for the interfacial friction coefficient, μ. We recently offered a simple alternative for reciprocating contacts [28]; mathematically, the friction coefficient is exactly equal to the difference in the forward and reverse tangential force divided by twice the average vertical force, or

$$\mu = \frac{F_{X\mathrm{f}} - F_{X\mathrm{r}}}{2 \cdot F_{Z\mathrm{ave}}} \tag{2}$$

where *X* denotes the tangential direction and *Z* denotes the vertical direction of the force transducer. In this way, the measurements of this tribometer are insensitive to *Y*-axis misalignment. Misalignments about the *X* and *Z* directions produce simple cosine errors which vanish for typical small angles.

A piezoelectric stage with direct capacitive metrology and positional feedback control provides reciprocating motion with traverse lengths from 0 to 1500 µm (±0.3 µm) and speeds from 0 to 5 mm/s. A vertical piezoelectric stage with direct capacitive metrology and closed loop control is used to load and unload the sample. The actuation range is 0–50 µm (±10 nm) and speeds from 0 to 0.2 mm/s. A manual vertical actuation stage enables coarse motion for probe positioning.

The spherical probes were permanently adhered to steel alignment shims prior to the experiments using an inert adhesive (not shown). The shim was mounted to the cantilevered load flexure with cyanoacrylate adhesive. The cantilevered beam is mechanically fixed to the vertical stage. Deflections of the flexure in the *X* and *Z* direction due to the forces of contact are measured using capacitance sensors with approximately 5 nm resolution. The force transducers were calibrated with mass standards known to ±100 nN.

2.3 Contact Radius Measurement

The measurement methods are illustrated in Fig. 2. A coarse manual stage is used to bring the probe to within a few microns of the cartilage surface. The vertical piezoelectric stage is commanded to move downward at 0.5 µm/s; the stage position and spring compression are measured during the approach at 10 kHz. The spring first deflects when the probe makes contact at z_0. Stage displacements are taken relative to z_0. The normal force is equal to the product of spring deflection and spring constant which was calibrated prior. As the stage continues downward, the penetration depth, δ_s, is the difference between the relative stage position and spring compression; $\delta_s = z - z_0 - \Delta L(z)$.

The contact radius, *a*, plays an important role in tribology; it is particularly important in cartilage tribology where fluid pressure increases with increased distance of

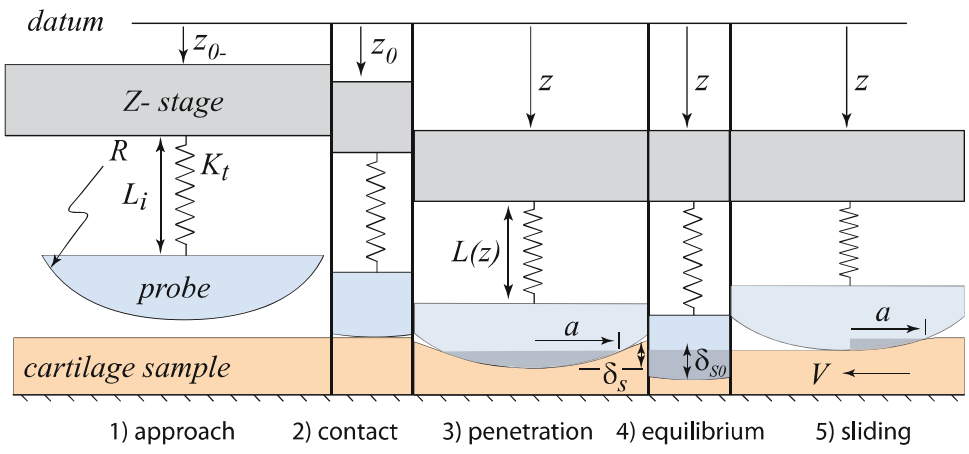

Fig. 2 Illustration of the testing procedure. The stage and spring displacements are measured directly with independent capacitive displacement sensors. The signals from the internal stage sensors are recorded and used for feedback controlled stage positioning

fluid flow (to regions of zero pressure). The Hertz and Winkler models relate the contact radius directly to the penetration depth, δ_s [29]. The Winkler model uses pure geometric interference and assumes that the cartilage layer behaves as a bed of independent springs; the displacement gradient is discontinuous at the edge of contact in this model. The Hertz solution is continuous but based on an assumption of an isotropic semi-infinite elastic solid. Hayes et al. [30] developed elasticity solutions to compensate for finite layer thickness. The contact radius here is smaller than the thickness and the Hertz model is used directly for simplicity. The Hertz model gives the following contact relationship:

$$a = \sqrt{R \cdot \delta_s} \tag{3}$$

It should be noted that Eq. 3 is still just a model and neglects effects from adhesion, nonlinearity, heterogeneity, thickness, etc. It does, however, provide a robust measure of relative changes in contact radius.

2.4 Friction Coefficient Measurement

Following indentation, the z-stage is maintained at full extension (50 μm) and the system is left to equilibrate over time as pressurized fluid escapes the contact zone; the equilibrium force and penetration depth are used to determine equilibrium modulus defined using the following Hertz formula;

$$E_0 = \frac{3 \cdot F_{n0} \cdot R^{-0.5} \cdot \delta_{s0}^{-1.5}}{4} \tag{4}$$

where the subscript, 0, denotes equilibrium. Subsequently, the horizontal stage is commanded to reciprocate along a 1500 μm long path (the input is a sine wave with a mean of 0 μm and amplitude of 750 μm). Data are collected for a speed range from 0.05 to 5 mm/s. Only data from the middle 20 μm of the sliding path are analyzed since the surface contact reference was obtained at $X = 0$ μm (the analysis area is $X = 0 \pm 10$ μm, where $X = 0$ is the indentation location). The velocity is constant over the analysis region.

3 Results

Figure 3 illustrates the testing and analysis procedures. To the left, the normal force, F_n, is plotted versus time for the first 600 s of an experiment with a 3.2 mm radius stainless steel probe. While the probe was out of contact and at the center of the wear track, the stage was commanded to move 50 μm toward the surface at a rate of 0.5 μm/s. Contact occurred after 3 μm of stage travel. As the stage continued downward (z), the normal force increased. Although biphasic theory effectively describes the uniaxial response of cartilage, poroelastic analogues to the Hertz contact solutions have yet to be established. An effective elastic modulus, E', is defined here with a quasi-static application of the Hertz solution:

$$E' = \frac{3 \cdot F_n \cdot R^{-0.5} \cdot \delta_s^{-1.5}}{4} \tag{5}$$

where normal force, radius and penetration depth are instantaneous rather than equilibrium values. The effective modulus is not an intrinsic material property; rather its definition, not unlike the definition of modulus for a composite material, is a useful engineering concept. Just as the modulus of a composite material depends on the moduli of the constituents, volume fractions, orientations and the interfacial shear strength between constituents, the effective modulus of cartilage under Hertzian contact is expected to depend on aggregate modulus, permeability, deformation rate, penetration depth, and effective probe radius. During indentation with a rate of 0.5 μm/s, the average effective modulus was 3.0 MPa. The effective modulus increases with increased penetration rate (up to 100 μm/s).

The stage reached its final position of 50 μm after 100 s. In the absence of a deformation rate, the normal force decreased and the penetration depth increased as the fluid evacuated the contact. The normal force equilibrated at 26 mN at a corresponding effective modulus of $E_0 = 1.38$ MPa; the standard deviation was $\sigma(E_0) = 0.002$ MPa but the experimental uncertainty was $u(E_0) = 0.04$ MPa (determined by the Law of Propagation of uncertainty [27, 31]). The uncertainty in normal force dominates the measurement uncertainty. By definition, fluid pressure is absent at equilibrium; consequently, the equilibrium modulus reflects a material property and will be denoted E_0. The aggregate modulus, H_a, is a material property defined as the ratio of equilibrium stress and equilibrium strain in uniaxial compression. Equilibrium and aggregate moduli are related in the following way for a linearly elastic isotropic material: $E_0 = \frac{H_a}{1-\upsilon^2}$. A Poisson's ratio of 0.4 gives $H_a = 1.15$ which is reasonably consistent with values from the literature which typically range from 0.5 to 1 MPa [5, 26]. Some recent studies suggest $\nu \sim 0$ [32] in which case $E_0 = H_a$. However, it should be noted that cartilage is neither isotropic nor linearly elastic.

At 525 s, the horizontal stage began reciprocating at 5 mm/s. The response to this imposed motion is immediate and significant; the normal force nearly tripled in magnitude while the penetration depth was cut in half. The effective modulus increased from 1.38 to 11.89 MPa. The mechanism responsible for this phenomenon is the same mechanism responsible for fluid load support during indentation; as Ateshian points out, pressurization occurs

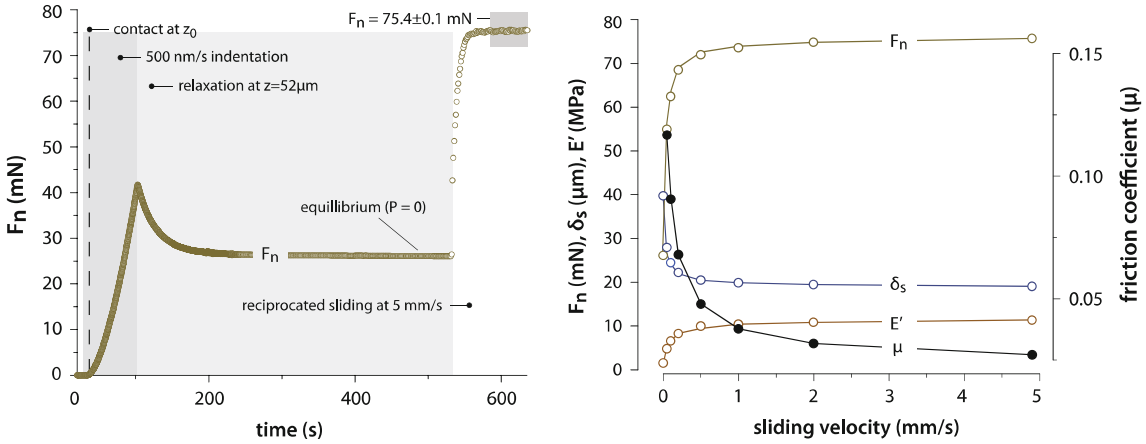

Fig. 3 *Left* Illustration of the methods: normal force versus time for a 440C stainless steel 3.2 mm radius sphere mated against bovine cartilage. The experimental uncertainty in normal force is 0.2 mN. Prior to loading, the probe is manually positioned to within 2–5 μm of the cartilage surface. The vertical stage is actuated 50 μm downward at 0.5 μm/s at a time of 0 s. The probe made contact at 3 μm and the stage reached its final position of 52 μm after 100 s where a peak force of 41.6 mN was obtained. The normal force decays as the pressurized fluid evacuates the contact. At equilibrium, only elastic deformations of the solid matrix support the load. At 525 s, the horizontal stage is commanded to reciprocate 1.5 mm in each direction at 5 mm/s whereby the normal force increases dramatically to 75.4 mN in response. *Right*: average values of normal force, penetration depth, elastic modulus, and friction coefficient plotted versus sliding speed. The standard deviation at each point is smaller than the corresponding data label

when the deformation velocity is faster than the diffusive velocity [7]. In other words, the sliding probe must move the cartilage and the resident fluid out of its way; a pressure gradient is required to drive the fluid at the necessary flow rate. The deformation velocity is the sliding speed (5 mm/s in this case). An imposed sliding deformation at the equilibrium penetration depth produces pressure and net lift. The penetration depth and contact area decrease until the system equilibrates.

The practical definition of the effective elastic modulus enables analysis of hypothetical events. In these experiments, normal force and penetration depth equilibrate together; i.e., neither load nor penetration depth is constant. Increased normal force and decreased penetration attenuate each other. Consider the following thought experiments where sliding is initiated under either constant load or constant penetration conditions. If the normal force were to be held constant at $F_n = 26$ mN, Eq. 5 predicts a reduction in penetration depth from 40 μm at equilibrium (i.e., without sliding) to 9 μm at 5 mm/s. On the other hand, if penetration depth were held constant at 40 μm, Eq. 5 predicts an increase in normal force from 26 mN at equilibrium to 226 mN at 5 mm/s. These changes are striking considering the relatively slow speeds of the experiments in comparison to physiological conditions during activity (on the order of 10 mm/s). Similar analyses could be useful for studying realistic joints under Hertzian contact conditions. These simple thought experiments highlights the role of sliding on the load bearing and lubrication mechanisms of articular cartilage in the body; the hydrated cartilage becomes a more effective bearing under sliding and impact conditions where typical materials are most likely to incur damage.

After maintaining a set of equilibrium conditions for 100 s, the sliding speed was reduced. The experiments were continued down to a minimum sliding speed of 0.05 mm/s. At each speed, the averages and standard deviations of the normal force, penetration, contact radius, sliding speed, friction coefficient, and effective modulus were computed. The data for the 3.2 mm radius pin are given in Table 1 and dependent variables are plotted versus sliding speed in Fig. 3. The normal force was insensitive to sliding speed from 5 to 0.05 mm/s. This result is consistent with the notion that load support increases with *Pe*. As the speed decreased, the material became effectively softer and the contact area increased. Because *Pe* is proportional to the product of speed and contact radius, the effect of increased radius partially nullifies the effect of reduced speed on normal force. It is only at low speeds (0–0.2 mm/s) that substantial load support is lost with reduced speed. This trend is particularly interesting considering that these speeds and contact radii are orders of magnitude lower than those found in vivo (Table 2).

The increase in friction coefficient was less abrupt than the decrease in normal force with decreased speed. A similar friction trend was found by Caligaris et al. [21]. Prior works had shown that (1) fluid load support depends on the Peclet number and (2) there is a direct relationship between fluid load support and friction coefficient [19, 23, 24]. Based on these studies, Caligaris et al. suggested that friction coefficient is also dominated by *Pe* [21]. This hypothesis was further supported by a prior AFM study for

Table 1 Average and standard deviation results for contact and sliding mechanics experiments with bovine articular cartilage in PBS

Command speed (mm/s)	F_n (mN)	δ_s (μm)	a (μm)	V (mm/s)	μ	E^* (MPa)
5	75.4 ± 0.1	19.3 ± 0.1	247.2 ± 0.3	4.90 ± 0.19	0.0272 ± 0.0006	11.89 ± 0.07
2	74.5 ± 0.1	19.7 ± 0.04	249.9 ± 0.2	2.00 ± 0.01	0.0317 ± 0.0003	11.37 ± 0.05
1	73.5 ± 0.1	20.1 ± 0.02	252.7 ± 0.1	1.00 ± 0.01	0.0377 ± 0.0005	10.84 ± 0.03
0.5	72.0 ± 0.1	20.8 ± 0.04	256.7 ± 0.4	0.50 ± 0.00	0.0479 ± 0.0007	10.14 ± 0.04
0.2	68.3 ± 0.03	22.3 ± 0.02	266.3 ± 0.2	0.20 ± 0.00	0.0680 ± 0.0002	8.61 ± 0.02
0.1	62.7 ± 0.1	24.7 ± 0.03	280.2 ± 0.3	0.10 ± 0.00	0.0906 ± 0.0002	6.78 ± 0.02
0.05	54.7 ± 0.1	28.2 ± 0.05	299.1 ± 0.4	0.050 ± 0.000	0.1168 ± 0.0014	4.87 ± 0.02
0.00	26.1 ± 0.02	39.9 ± 0.01	356.0 ± 0.1	N/A	N/A	1.38 ± 0.00

The cartilage explant was from the lateral femoral condyle of a 12–20 month animal. The 440C stainless steel probe had a 3.2 mm radius

Table 2 Average and standard deviation results for contact and sliding mechanics experiments with bovine articular cartilage in PBS

Command speed (mm/s)	F_n (mN)	δ_s (μm)	a (μm)	V (mm/s)	μ	E^* (MPa)
5	43.4 ± 0.1	23.75 ± 0.05	137.3 ± 0.0	4.87 ± 0.20	0.0251 ± 0.0006	10.86 ± 0.06
2	46.18 ± 0.05	24.23 ± 0.03	138.7 ± 0.0	2.00 ± 0.00	0.0296 ± 0.0002	10.31 ± 0.03
1	44.85 ± 0.04	24.83 ± 0.02	140.4 ± 0.0	1.00 ± 0.01	0.0365 ± 0.0003	9.65 ± 0.02
0.5	42.85 ± 0.03	25.71 ± 0.02	142.9 ± 0.0	0.499 ± 0.00	0.0484 ± 0.0003	8.75 ± 0.02
0.2	38.01 ± 0.04	27.78 ± 0.02	148.5 ± 0.0	0.20 ± 0.00	0.0723 ± 0.0004	6.91 ± 0.02
0.1	31.91 ± 0.04	30.39 ± 0.02	155.3 ± 0.0	0.10 ± 0.00	0.0978 ± 0.0005	5.07 ± 0.01
0.05	24.86 ± 0.05	33.37 ± 0.02	162.8 ± 0.0	0.050 ± 0.000	0.1337 ± 0.0016	3.43 ± 0.01
0.00	9.11 ± 0.02	39.67 ± 0.01	177.4 ± 0.1	N/A	N/A	0.97 ± 0.00

The 440C stainless steel probe had a 0.8 mm radius

which Pe was less than 1 and only equilibrium friction ($\mu = 0.2$) was detected [25]. In both cases the contact radius was assumed constant with varying speed.

3.1 Effect of Probe Radius

The equilibrium modulus of cartilage against the 0.8 mm radius probe was found to be 0.97 MPa; although $\sigma(E_0) < 0.01$, it should be noted that the uncertainty in this value is approximately 0.06 MPa. E_0 for the smaller probe was approximately 30% lower than it was against the larger probe. This trend has since been reproduced for two additional samples. The Hertz model assumes a semi-infinite isotropic elastic solid which is clearly not the case for cartilage. Although the contact radius is significantly smaller than the cartilage thickness, the bone substrate will have a stiffening effect on larger contacts which becomes very important in the body [30].

The effective modulus was a strong function of sliding speed for both probes and became particularly sensitive at low speeds. At any given speed, the smaller probe produces a significantly lower modulus which suggests that modulus increases with both velocity and probe radius. The elastic modulus is plotted versus Pe in Fig. 4. Aggregate modulus, H_a, and permeability, k, are assumed to be 1 MPa and 0.001 mm^4/Ns, respectively, based on prior literature [5]. As others have pointed out, k may decrease with increased deformation. Although the curves are distinct, the effective modulus appears to be dependent on the product of speed and contact radius rather than speed alone. Friction coefficient is plotted versus sliding speed on a log scale for both probe radii in Fig. 4. Based on the hypothesis from Caligaris et al. that friction coefficient is dependent on Pe, higher friction would be expected for the small probe (due to reduced contact radius) at any speed. At 0.5 mm/s and above, the friction coefficient of cartilage was virtually identical for the 3.2 and 0.8 mm radius probes despite the factor of four differences in contact area.

Interestingly, while factor of two changes in velocity induced a marked frictional response, factor of four changes in probe radius produced little effect, especially at high speed. In varying probe radius from a bovine condyle ($\sim$20 mm) to a 6.5 mm radius lens, Caligaris et al. [21] did find a trend of increased friction with decreased radius. However, the trend was comparable in magnitude to the error bars. As a result, the authors could neither support nor refute the hypothesized role of contact radius. We varied the normal force from 20 to 200 mN during sliding at

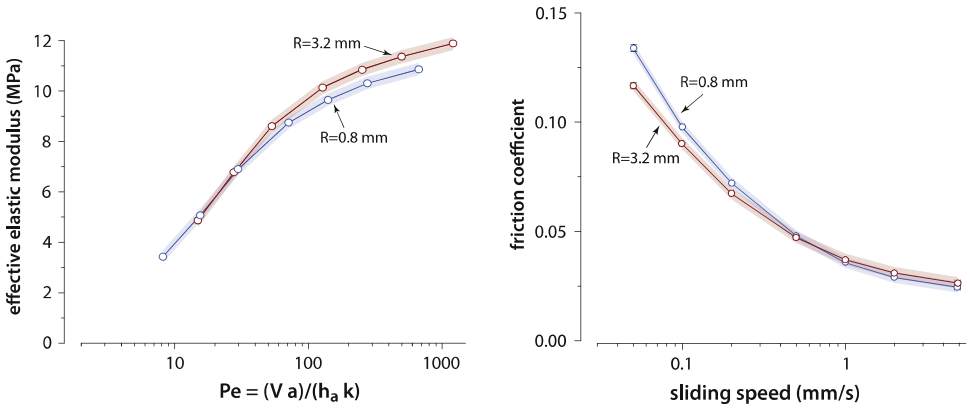

Fig. 4 *Left* effective elastic modulus plotted versus the Peclet number for 3.2 and 0.8 mm probes. *Right* friction coefficient plotted versus sliding speed for 3.2 and 0.8 mm probes. The *shaded regions* represent the 95% confidence intervals based on the larger of the standard deviation and experimental uncertainty. The data suggest that the elastic modulus depends on the product of speed and contact radius (Peclet number), while the friction coefficient depends on speed alone

5 mm/s as a means to vary contact radius at a given location, probe radius, and speed. The friction coefficient remained constant over the entire load and contact area ranges (data not shown). While friction coefficient is clearly sensitive to speed, we have found no evidence that it is strongly influenced by load, probe radius or contact radius.

4 Discussion

4.1 Role of Fluid Shear

Engineers take every precaution to eliminate solid contacts which are known to produce considerable friction and wear. Consequently, early hypotheses for cartilage lubrication largely utilized fluid film mechanisms of contact avoidance. The measured friction forces and contact areas suggest shear stresses that are significantly larger than one would expect from water behaving as a Newtonian fluid. Given the room temperature viscosity of water, $\eta = 0.8 \times 10^{-6}$ mN s/mm^2, the sliding velocity, V, and the average shear stress (friction force divided by area) at each condition, the definition of a Newtonian fluid $\left(\tau = \eta \cdot \frac{V}{t}\right)$ indicates that the film thickness ranges from 0.001 to 0.1 nm. Even these estimates are grossly conservative given the porosity of the surface. As McCutchen [4] points out, the interface becomes analogous to a solid if the fluid film approaches nanometer thickness. The boosted theory of friction suggests that extremely viscous gels are left at the interface following the removal of water from the synovial fluid. These studies were done with PBS and there is no reason to believe that the content of the lubricant or the pressures involved would yield anything significantly more viscous than water. It can therefore be concluded that friction from fluid shear was negligible in these measurements. Ateshian [33] has previously suggested that cartilage friction is dominated by shear of the infrequent solid–solid contacts. Improved fundamental understanding of cartilage lubrication requires an improved understanding of these solid–solid interactions.

4.2 Implications of the Internal Structure

The normal force can be resolved into components due to elastic deformation and fluid pressure. As with traditional composite materials, the distribution of stresses between matrix and filler (fluid) varies dramatically with internal structure. For example, the composite in Fig. 5a is called an equal stress structure because the filler and matrix carry equal stress. Either the filler or matrix can reside at the surface. In the case shown, the friction is entirely due to fluid shear and the forces would be significantly lower than those observed (as shown above). Conversely, when the solid is at the interface it always supports a stress P. When P increases, the contact area decreases in proportion to the increase in shear stress; the net result is independence of the observed friction coefficient on fluid pressure. Hence, this structure cannot explain well-established phenomena of cartilage lubrication.

The equal strain structure shown in Fig. 5b can explain lubrication of cartilage. As the surface is displaced, the strain is constant throughout. In a traditional composite material, the filler and matrix have high and low moduli, respectively. For a given strain, the filler carries significantly higher stress and effectively shields the soft matrix. The founding premise behind the most current hypothesis of cartilage friction is that hydrostatic fluid pressure can support a significant fraction of the total normal force (possibly 90–99% in vivo) [7].

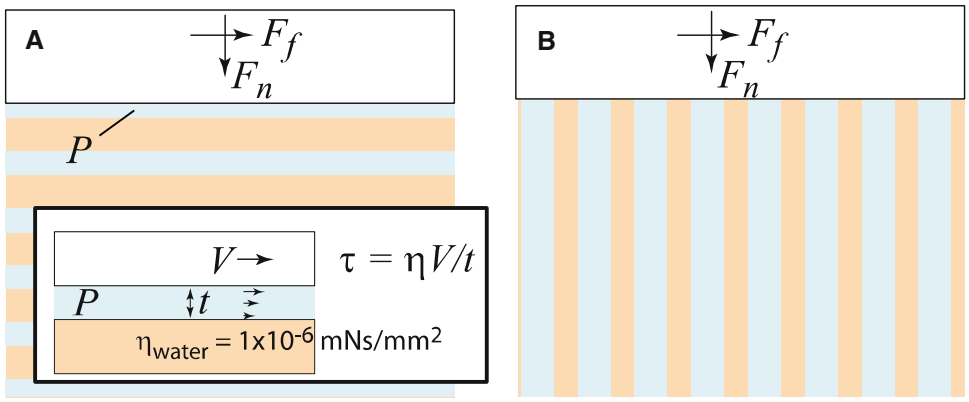

Fig. 5 Schematics of theoretically bounding composite structures: **a** equal stress structure; **b** equal strain structure. The load is shared equally by the filler and matrix in the equal stress structure. The filler can support the majority of the load in the equal strain structure. In the most current hypothesis for cartilage lubrication, the normal and traction stresses on the matrix are limited via preferential load support by the fluid. The cartilage structure is a three-dimensional fluid network that behaves more like **b**

Idealized equal stress and equal strain models are bounding structures, and most systems, including cartilage, lie somewhere in between; the critical question is whether or not cartilage can be approximated by the equal strain model. A hypothetical model of the three-dimensional structure and the resulting pressure distribution on the probe surface is illustrated in Fig. 6. McCutchen [4] recognized that pockets of pressurized fluid beneath a solid contact tend to increase the interfacial stresses on the matrix. The more pressure influences the matrix stress, the closer the structure gets to the equal stress model and the less efficient the bearing.

In 1997, Ateshian [24] proposed a cartilage friction model which treated fluid pressure and matrix normal stress independently; the treatment implies an equal strain structure. The aggregate modulus is the proportionality between stress and strain in the absence of fluid pressurization and is a fundamental property of the elastic matrix. Compression measurements taken during a friction experiment were used to determine the elastic strain (which is lower at a given load when the fluid is pressurized). The product of aggregate modulus and strain represents the apparent stress carried by the elastic matrix. The actual elastic stress and pressure can be determined if the porosity, or area fraction of the matrix is known. The fact that porosity is unknown has no bearing on the conclusions drawn from the analysis.

In 1998, the group modified the analysis to account for the effect of hydrostatic pressure on the elastic stress at the interface [33]. In this model, $\mu_{\text{eff}} = \mu_{\text{eq}}\left(1-(1-\varphi)\frac{W_{\text{p}}}{W}\right)$ where μ_{eff} is the effective friction coefficient or ratio of friction force and total normal force, φ is the 'porosity', W_{p} is the load carried by fluid pressure, and W is the normal force. The modifier, φ, accounts for the structural effect of pressure on elastic stress. When $\varphi = 0$, the model is equivalent to their 1997 model which is equivalent to the equal strain structure shown in Fig. 5b. In this case $\mu_{\text{eff}} = \mu_{\text{eq}}\left(1-\frac{W_{\text{p}}}{W}\right)$. When the fluid supports no load, the effective friction coefficient is equal to the equilibrium

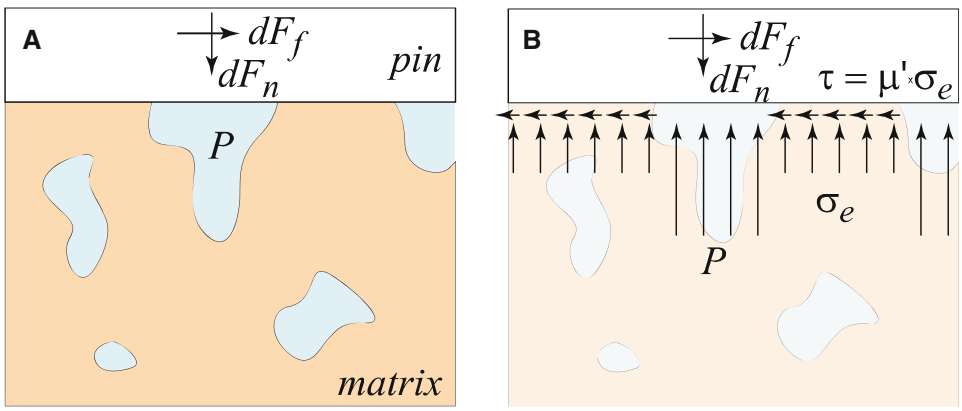

Fig. 6 **a** A differential segment of the cartilage-probe contact; **b** illustration of the hypothetical stress distributions that balance the applied forces. Fluid pressure is significantly greater than the matrix normal stress as depicted. Fluid shear is assumed negligible, so the differential friction force is the product of the interfacial friction coefficient, matrix stress, and matrix contact area

friction coefficient; when the fluid supports the entire load the effective friction coefficient is equal to zero. When $\varphi = 1$, this model is identical to the equal stress model and the effective friction coefficient is always equal to the equilibrium friction coefficient.

McCutchen [34] studied this effect 30 years ago by varying the hydrostatic pressure in a vessel containing the friction experiment; the pressure had no effect on the observed friction coefficient. Krishnan et al. [19] directly measured the fluid pressure, normal force and friction force during uniaxial confined compression experiments which enabled the group to determine the equilibrium friction coefficient and φ from linear regression of a thorough dataset. The group found that $\varphi = 0.017 \pm 0.063$. Both of these studies confirmed that elastic stress is nearly independent of fluid pressure and indicates that cartilage is a three-dimensional equal strain structure to an excellent approximation. The structure of cartilage has been optimally designed to minimize the matrix stress and friction force for a given set of conditions.

Since the fluid pressure and elastic stress may be treated independently with high confidence, the elastic contribution to the normal force may be determined for any test condition if the probe radius, instantaneous penetration depth, and equilibrium modulus are known. Under the stationary contact, the fluid pressure subsides over time leaving only the elastically deformed matrix to support the normal force at equilibrium. Equation 4 is used with the probe radius, equilibrium force and penetration depth to determine the equilibrium modulus. This method assumes that the modulus is independent of indentation depth (since modulus is determined from an equilibrium depth that is different than the depth of interest). We have since measured equilibrium modulus with penetration depths from 10 to 100 μm and confirmed that modulus is independent of depth in that range.

As the cartilage moves through the contact, the matrix is deformed and fluid is displaced leaving no material for load support behind the pin (as depicted in the 'sliding' regime of Fig. 2). Although cartilage has a time-dependent recovery following deformation, the time constant is on the order of 100 s under these conditions (Fig. 3). Here it is reasonably assumed that the trailing half of the contact is unable to provide meaningful load support; i.e., it is assumed here that only the front half supports normal load. The elastic force component, F_e, is:

$$F_e = \frac{4 \cdot E_0 \cdot R^{0.5} \cdot \delta_s^{1.5}}{6} \tag{6}$$

where E_0 is the measured equilibrium modulus, R is the probe radius, and δ_s is the penetration depth. The pressure force component, F_p, is the difference between the total normal force and the elastic force component. The fluid

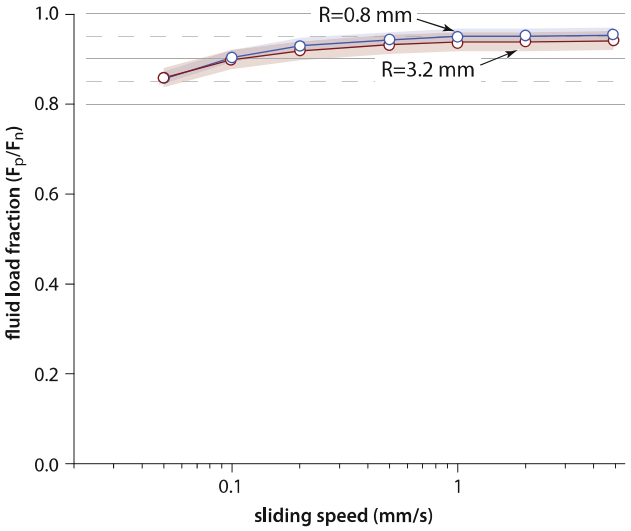

Fig. 7 Fluid load fraction plotted versus sliding speed from 0.05 to 5 mm/s for 3.2 and 0.8 mm probes. The *shaded regions* represent the 95% confidence intervals; this is based on the standard deviations since they were larger than the measurement uncertainties

load fraction, defined as F_p/F_n (equivalent to W_p/W from Ateshian et al. [24, 33]), is plotted versus sliding speed for both probe radii in Fig. 7. The results are striking considering the trends from the uniaxial compression literature which indicates strong sensitivity to contact radius. The fluid load support fraction was unexpectedly insensitive to speed, probe radius and contact radius. Both probes supported better than 85% of the normal force down to 0.05 mm/s where speed and contact radius are at least an order of magnitude smaller than they would be during activity in vivo. It should also be noted that trend is independent of the assumption that the rear of the contact supports none of the normal load. Hypothetically, if the cartilage did recover quickly enough to support the entire area ($A = \pi a^2$), the elastic contribution would simply double; i.e., fluid load support would always exceed 70% and would be similarly insensitive to speed and probe radius.

Ateshian has suggested that cartilage friction results primarily from shear of solid–solid contacts. Further, they experimentally validated their friction model by demonstrating that the friction coefficient increased proportionally as the fluid load support decreased [19]. It should be noted that the measurements were collected with a stationary contact where fluid escapes, pressure subsides, and friction increases from low initial values to higher equilibrium values when matrix supports the entire load. The results of this study show a similar dependence albeit over a very limited fluid load support range from 85 to 95%. More interesting is the impact of apparent contact area. Friction coefficient is plotted versus apparent contact area

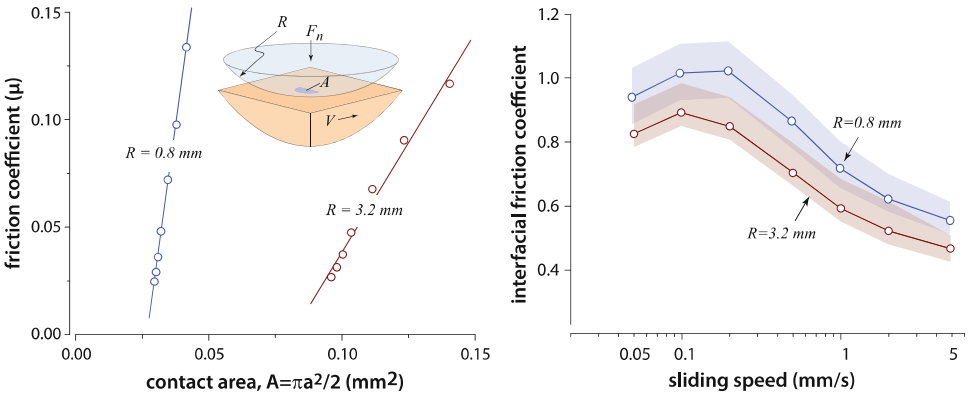

Fig. 8 *Left* friction coefficient plotted versus apparent contact area, *A*. For both probes, the friction coefficient was approximately proportional to contact area. *Right* interfacial friction coefficient plotted versus sliding speed. The interfacial friction coefficient is equal to the measured friction coefficient divided by the fraction of the normal load supported by the matrix

in Fig. 8. Friction coefficient is approximately proportional to the contact area for both probe radii.

The interfacial friction coefficient, a concept derived from the seminal work of Bowden and Tabor during the development of the adhesive theory of friction [35, 36], is more fundamentally significant than the traditional definition which can encompass various phenomena; it is defined here as the ratio of the elastic shear force to elastic normal force.

$$\mu' = \frac{F_{\mathrm{fe}}}{F_{\mathrm{ne}}} \tag{7}$$

The elastic normal force is the normal force component supported by the elastic matrix. The elastic shear force is equal to the measured friction force if other contributions are negligible.[1] The interfacial friction coefficient is plotted versus sliding speed on the right of Fig. 8; the shaded regions represent the 95% confidence intervals. Three interesting trends were observed. (1) The interfacial friction coefficient is dependent (albeit weakly) on the probe radius. The normal force per unit area is higher for the smaller probe[2] and the interfacial friction coefficient may be a function of stress (although μ typically decreases with increased stress). Although the plowing components to friction (due to normal pressure components in the frictional direction) cannot be determined without known pressure distributions, it can be concluded that the plowing friction coefficient of the smaller probe is twice that of the larger probe. The size dependence may be due to the disproportionate contribution of plowing to the friction of the small probe. (2) The friction coefficient is a complicated, but systematic function of the sliding speed. In the model, it was assumed that fluid pressure and elastic properties are completely independent. The trend suggests reduced shear stress across solid contacts at higher pressures. A possible, if not likely, explanation is the penetration of pressurized fluid into the 'solid' contact periphery. In such cases, the periphery would support load without significant shear. This effect would increase with pressure. At slower speeds, the interfacial friction coefficients reach maxima and begin to decrease with decreased speed. It was considered that damage and realignment could be responsible; for example, this is the mechanism responsible for reduced friction of Polytetrafluoroethylene (PTFE, Teflon®) following an initial sliding contact event. Changes over time were not observed as would be expected during damage or realignment processes; it is more likely that the trend is due to a competition between improved lubrication at high speeds and intrinsic velocity dependence of the solid interface. Many polymers exhibit speed-dependent friction. The friction coefficient of PTFE, for example, increases from 0.05 to 0.3 when speed is increased from about 1 to 100 mm/s [37]. (3) The magnitude of the interfacial friction coefficient is unexpectedly high ranging from 0.4 to 1.1. Such values are not without precedence; McCutchen [4] found that the friction coefficient of cartilage continues to rise to values well above 0.3 after long periods of time in a stationary contact with water, PBS and synovial fluid lubricants. We studied (2) and (3) by intentionally removing the lubricant from the reservoir during sliding. Low friction and load support were sustained for 5–20 min whereby subsequent sliding led to monotonically decreased load and increased friction coefficient. During this period of 'dry' sliding (the cartilage was hydrated not saturated), the friction coefficient increased markedly with increased speed and decreased markedly with decreased speed. Additionally, the friction coefficient increased to values well above 1 when given enough time ($\sim$1 h).

[1] There is strong evidence that fluid shear is negligible. The plowing contribution depends on the known deformation geometry and the unknown pressure distributions. Based on the deformed geometry, it can be concluded that the plowing friction component from the small probe is approximately twice that of the large probe. Because plowing increases the friction of the smaller probe disproportionately, the similar frictional responses suggest a limited contribution from plowing.

[2] Assuming 70% water, 30% matrix, the matrix stresses are estimated at 120 and 180 kPa for the 3.2 and 0.8 mm radii, respectively, during sliding; they are 340 and 440 kPa under static loading. At 5 mm/s, the hydrostatic pressures are 1.1 and 2.2 MPa for the 3.2 and 0.8 mm radii, respectively.

5 Closing Remarks

This work has provided the following notable findings:

(1) The fluid load support was greater than 85% for all sliding conditions (0% fluid support when $V = 0$) and was insensitive to both probe radius and sliding speed.
(2) Low sustainable friction coefficients ($\mu = 0.025$) were observed beneath localized contacts. Reducing the probe and contact area by a factor of approximately 4 had little effect on fluid pressurization or friction coefficient.
(3) The friction coefficient was proportional to contact area for both probes over the entire speed range from 0.05 to 5 mm/s.
(4) The contact area is a strong function of the probe radius and sliding speed. For a given probe, decreased speed reduces the pressure gradient which requires larger contact radii to support reduced normal force.

The findings were consistent with the adhesive theory of friction; as speed increases, increased effective hardness reduced the area of solid–solid contact which subsequently reduced the friction force. Contrary to typical engineering applications where damage is more probable under impact and high speed conditions, the results suggest that joint motion is actually beneficial for maintaining low matrix stresses, small contact areas, and effective lubrication. The results demonstrate effective pressurization and lubrication beneath single asperity microscale contacts. With carefully designed experimental conditions, local friction probes can facilitate more fundamental studies of cartilage lubrication, friction, and wear, and potentially add important insights into the mechanical mechanisms of OA.

Acknowledgment The project described was supported by NIH grants (P20-RR016458 and AR054385).

References

1. Murphy, L., Schwartz, T.A., Helmick, C.G., Renner, J.B., Tudor, G., Koch, G., Dragomir, A., Kalsbeek, W.D., Luta, G., Jordan., J.M.: Lifetime risk of symptomatic knee osteoarthritis. Arthritis Rheumatism-Arthritis Care Res. **59**, 1207–1213 (2008)
2. Lane, N.E., Buckwalter, J.A.: Exercise—a cause of osteoarthritis. Rheum. Dis. Clin. North Am. **19**, 617–633 (1993)
3. Mow, V.C., Ateshian, G.A., Spilker, R.L.: Biomechanics of diarthroidal joints—a review of 20 years of progress. J. Biomech. Eng. **115**, 460–467 (1993)
4. McCutchen, C.W.: The frictional properties of animal joints. Wear **5**, 1–17 (1962)
5. Mow, V.C., Kuei, S.C., Lai, W.M., Armstrong, C.G.: Biphasic creep and stress-relaxation of articular-cartilage in compression—theory and experiments. J. Biomech. Eng. **102**, 73–84 (1980)
6. Park, S.H., Krishnan, R., Nicoll, S.B., Ateshian, G.A.: Cartilage interstitial fluid load support in unconfined compression. J. Biomech. **36**, 1785–1796 (2003)
7. Ateshian, G.A.: The role of interstitial fluid pressurization in articular cartilage lubrication. J. Biomech. **42**, 1163–1176 (2009)
8. Wright, V., Dowson, D.: Lubrication and cartilage. J. Anat. **121**, 107–118 (1976)
9. Dowson, D., Wright, V., Longfield, M.D.: Human joint lubrication. Biomed. Eng. **4**, 160–165 (1969)
10. Macconaill, M.A.: The function of intra-articular fibrocartilages, with special reference to the knee and inferior radio-ulnar joints. J. Anat. **66**, 210–227 (1932)
11. McCutchen, C.W.: Sponge-hydrostatic and weeping bearings. Nature **184**, 1284–1285 (1959)
12. Charnley, J.: How our joints are lubricated. Triangle **4**, 175–179 (1960)
13. Schmidt, T.A., Gastelum, N.S., Nguyen, Q.T., Schumacher, B.L., Sah, R.L.: Boundary lubrication of articular cartilage—role of synovial fluid constituents. Arthritis Rheum. **56**, 882–891 (2007)
14. Barnett, C.H., Cobbold, A.F.: Lubrication within living joints. J. Bone Joint Surg. **44**, 662–674 (1962)
15. Little, T., Freeman, M., Swanson, S.A.V.: Experience on friction in the human hip joint. In: Wright, V. (ed.) Lubrication and Wear in Joints, pp. 110–114. Sector Publishing Ltd, London (1969)
16. Dowson, D.: Modes of lubrication in human joints. Proc. IMechE **181**, 45–54 (1967)
17. Maroudas, A.: Hyaluronic acid films. Proc. IMechE **181**, 122–124 (1967)
18. Walker, P.S., Dowson, D., Longfield, M.D., Wright, V.: "Boosted lubrication" in synovial joints by fluid entrapment and enrichment. Ann. Rheum. Dis. **27**, 512–520 (1968)
19. Krishnan, R., Kopacz, M., Ateshian, G.A.: Experimental verification of the role of interstitial fluid prezzurization in cartilage lubrication. J. Orthop. Res. **22**, 565–570 (2004)
20. Carter, M.J., Basalo, I.M., Ateshian, G.A.: The temporal response of the friction coefficient of articular cartilage depends on the contact area. J. Biomech. **40**, 3257–3260 (2007)
21. Caligaris, M., Ateshian, G.A.: Effects of sustained interstitial fluid pressurization under migrating contact area, and boundary lubrication by synovial fluid, on cartilage friction. Osteoarthritis Cartilage **16**, 1220–1227 (2008)
22. Bell, C.J., Ingham, E., Fisher, J.: Influence of hyaluronic acid on the time-dependent friction response of articular cartilage under different conditions. Proc. Inst. Mech. Eng. H **220**, 23–31 (2006)
23. Ateshian, G.A., Wang, H.Q.: A theoretical solution for the frictionless rolling-contact of cylindrical biphasic articular-cartilage layers. J. Biomech. **28**, 1341–1355 (1995)
24. Ateshian, G.A., Wang, H.: Rolling resistance of articular cartilage due to interstitial fluid flow. Proc. Inst. Mech. Eng. H **211**, 419–424 (1997)
25. Park, S., Costa, K.D., Ateshian, G.A.: Microscale frictional response of bovine articular cartilage from atomic force microscopy. J. Biomech. **37**, 1679–1687 (2004)
26. Setton, L.A., Mow, V.C., Muller, F.J., Pita, J.C., Howell, D.S.: Mechanical-properties of canine articular-cartilage are significantly altered following transection of the anterior cruciate ligament. J. Orthop. Res. **12**, 451–463 (1994)
27. Schmitz, T.L., Action, J.E., Ziegert, J.C., Sawyer, W.G.: The difficulty of measuring low friction: uncertainty analysis for friction coefficient measurements. J. Tribol. **127**, 673–678 (2005)
28. Burris, D.L., Sawyer, W.G.: Addressing practical challenges of low friction coefficient measurements. Tribol. Lett. **35**, 17–23 (2009)
29. Johnson, K.L.: Contact Mechanics. Cambridge University Press, Cambridge (1985)

30. Hayes, W.C., Herrmann, G., Mockros, L.F., Keer, L.M.: Mathematical-analysis for indentation tests of articular-cartilage. J. Biomech. **5**, 541–551 (1972)
31. Schmitz, T., Action, J., Burris, D., Ziegert, J., Sawyer, W.: Wear-rate uncertainty analysis. J. Tribol. **126**, 802–808 (2004)
32. Pawaskar, S.S., Fisher, J., Jin, Z.M.: Robust and general method for determining surface fluid flow boundary conditions in articular cartilage contact mechanics modeling. J. Biomech. Eng. **132**, 031001-1–031001-8 (2010)
33. Ateshian, G.A., Wang, H.Q., Lai, W.M.: The role of interstitial fluid pressurization and surface porosities on the boundary friction of articular cartilage. J. Tribol. **120**, 241–248 (1998)
34. McCutchen, C.W.: Lubrication of Joints, the Joints and Synovial Fluid. Academic Press, New York (1978)
35. Bowden, F.P., Tabor, D.: Friction and Lubrication of Solids. Clarendon Press, Oxford (1986)
36. Bowden, F.P., Tabor, D.: The area of contact between stationary and between moving surfaces. Proc. R. Soc. Lond. A Math. Phys. Sci. **169**, 0391–0413 (1939)
37. Mclaren, K.G., Tabor, D.: Visco-elastic properties and friction of solids—friction of polymers—influence of speed and temperature. Nature **197**, 856–859 (1963)